Symmetric Phase-Only Matched Filtering of Fourier–Mellin Transforms for Image Registration and Recognition

Qin-sheng Chen, Michel Defrise, and F. Deconinck, *Member, IEEE*

Abstract—**This paper presents a new method to match a two-dimensional image to a translated, rotated, and scaled reference image. The approach consists of two steps: the calculation of a Fourier–Mellin invariant (FMI) descriptor for each image to be matched, and the matching of the FMI descriptors. The FMI descriptor is translation invariant, and represents rotation and scaling as translations in parameter space. The matching of the FMI descriptors is achieved using a symmetric phase-only matched filtering (SPOMF).**

The performance of the FMI-SPOMF algorithm is the same or similar to that of the phase-only matched filtering when dealing with image translations. The significant advantage of the new technique is its capability to match rotated and scaled images accurately and efficiently. The innovation is the application of the SPOMF to the FMI descriptors, which guarantees a high discriminating power and an excellent robustness in the presence of noise.

This paper describes the principle of the new method and its discrete implementation for either image detection problems or image registration problems. Practical results are presented for various applications in medical imaging, remote sensing, fingerprint recognition, and multiobject identification.

I. Introduction

IMAGE MATCHING, defined as the problem of evaluating the similarity of objects in different images, is used to detect changes in a scene, estimate object motion, locate targets, identify objects, or integrate information from different types of images, etc. A matching algorithm should be robust with respect to low signal to noise ratio (SNR), and should be accurate even when the same object has different intensities or different orientations and sizes in the two images to be matched, or when the object is partially truncated in one of the images. Furthermore, a matching algorithm must be efficient numerically.

The most common approach to image matching is based on the cross-correlation technique, also referred to as template matching [1]–[8]. This technique is not ideal, however, because the auto-correlation function of natural images has significant values even at rather large distances. This means that the maximum of the cross-correlation between two images is rather broad, and therefore difficult to locate in the presence of noise [4]. Several alternatives to the cross-correlation function have been proposed, such as Venot's sign change criterion [9], [10]. All these techniques require the calculation of some kind of generalized correlation for all possible values of the parameters that characterize the geometric transform relating the two images. Such an exhaustive calculation is extremely time consuming when the geometric transforms relating the two images include not only a translation, but also a rotation angle and a scaling. This is why few researchers have used cross-correlation techniques to match rotated and scaled (dilated) images. Another group of image matching techniques are based on moments or moment invariants [11]–[18]. Since moments are very sensitive to noise, most matching algorithms have been applied to binary images (e.g., in character recognition) or to binarized gray value images, using only lower order moments. Abu-Mostafa and Psaltis found that matching based on moment invariants has a rather limited discriminating power [12], and Rusinek, Levy, and Noz also pointed out the poor performances of moment based techniques for the registration of medical image [19].

The importance of the phase of the Fourier transform (the spectral phase) in image reconstruction has systematically been demonstrated by Oppenheim and Lim [20]. Much efforts have been made to use phase information for image matching, particularly in optical image processing systems where analogue Fourier transforms can be achieved efficiently. Some well known matching techniques are based on phase-only matched filters [21] and variants [22]–[25], such as binary phase-only matched filters [23] and nonlinear matched filters [24], [25]. The advantages of these filters are their high discriminating power, numerical efficiency, and robustness against noise. A major drawback, however, is that the spectral phase of an image is not invariant for rotation and scaling. Hence, phase-only matched filtering is efficient only when the effects of the rotation and scaling are small and can be ignored [26]. When this is not the case, it becomes necessary to rotate and scale the image spectra and to calculate their correlation for every possible rotation angle and scale factor, as proposed by De Castro and Morandi in solving the rotation problem [27], [28]. An alternative efficient solution to the rotation problem was proposed by Hsu, Arsenault, and April using a circular harmonic expansion [29], [30], but these authors have pointed out the difficulty in locating a common rotation centre in the two images.

Manuscript received April 27, 1993; revised April 26, 1994. Recommended for acceptance by Associate Editor D. Daugman.

Q. Chen was with the Experimental Medical Imaging Lab., NUGE, AZ-VUB, Laarbeeklaan 101, B-1090, Brussels, Belgium. He is now with the Department of Medical Physics, Memorial Sloane-Kettering Cancer Center, New York, NY 10021 USA.

M. Defrise and F. Deconinck are with the Experimental Medical Imaging Lab., NUGE, AZ-VUB, Laarbeeklaan 101, B-1090, Brussels, Belgium.

IEEE Log Number 9405782.

Functions that are invariant under some of the allowed geometric transformations allow one to reduce the dimension of the parameter space in which the correlation quality figure must be optimized. One well known invariant function is the Fourier–Mellin transform (referred to here as Fourier–Mellin invariant (FMI) descriptor), which is translation-invariant and represents rotation and scaling as translations along the corresponding axes in parameter space [31]–[39]. All previous methods match the FMI descriptors using cross-correlation, or variants of cross-correlation. Since the Fourier–Mellin transform is based on the magnitude of the Fourier transform, the cross-correlation of the Fourier–Mellin transforms generally yields a very broad maximum, and this technique is therefore unreliable both for the identification and localization of an object in an image.

In this paper, we propose a two-dimensional matching technique based on the symmetric phase-only matched filtering of the Fourier–Mellin invariant descriptors of the images, and referred to as FMI-SPOMF. This new method combines the advantages of the symmetric phase-only matched filtering (sharpness of the correlation peak, robustness in the presence of noise) with the decoupling of rotation, scaling, and translation allowed by the FMI descriptors. This results in a sensitive and efficient technique for image matching, with significantly improved discriminating power and estimation accuracy compared to the methods proposed in [8], [34]–[37]. The new method is also robust for image truncation. The good performance of our FMI-SPOMF algorithm has been demonstrated for several practical applications.

This paper is organized in the following way. In the next section, we describe the classical matched filtering and the phase-only and symmetric phase-only matched filtering. The Fourier–Mellin invariant descriptor is defined in Section III. Section IV describes the FMI-SPOMF algorithm. The discrete implementation is discussed in Section V. The performance of the FMI-SPOMF algorithm for rotation and scaling are evaluated in Section VI. Section VII demonstrates some applications of the FMI matching to medical image registration, remote sensing image matching, fingerprint recognition, and multiobject identification. Finally, our conclusion is given in Section VIII.

II. Matched Filtering and Phase-Only Matched Filtering

The aim of image matching is either to determine the presence of a known image $r(x', y')$ in a noisy scene $s(x, y)$,

$$s(x, y) = r(x', y') + n(x, y), \tag{1}$$

or to determine the parameters $p_1, \cdots, p_n$ of a geometric transformation relating two images $\mathbf{s}$ and $\mathbf{r}$:

$$s(x, y) = r(x'(x, y, p_1, \cdots, p_n), y'(x, y, p_1, \cdots, p_n)) + n(x, y), \tag{2}$$

where the functions $x'(x, y, p_1, \cdots, p_n)$ and $y'(x, y, p_1, \cdots, p_n)$ define a geometric transformation depending on n parameters $p_1, \cdots, p_n$. In (1) and (2), $n(x, y)$ denotes a zero-mean, stationary random noise field that is independent of the signal $r(x, y)$.

In this section, we consider a simple two-dimensional translation problem with translation offset (x_o, y_o), thus, $x' = x - x_o, y' = y - y_o$. The Fourier transforms of the two images are defined by: $R(u, v) = \mathcal{F}\{r(x, y)\}$ and $S(u, v) = \mathcal{F}\{s(x, y)\}$ with $\mathcal{F}\{.\}$ denoting the Fourier transformation. The classical matched filter [40], [41], which maximizes the detection signal-to-noise ratio, has a transfer function

$$H(u, v) = \frac{R^*(u, v)}{|N(u, v)|^2} \tag{3}$$

where, $R^*(u, v)$ is the complex conjugate of the Fourier spectrum $R(u, v)$ and $|N(u, v)|^2$ is the noise power-spectral density. If the noise has a flat spectrum with intensity n_w, the transfer function of the matched filter reduces to

$$H(u, v) = \frac{1}{|n_w|^2} R^*(u, v) \tag{3'}$$

and the output of the filter is the convolution of $r^*(-x, -y)$ and $s(x, y)$:

$$q_o(x, y) = \frac{1}{|n_w|^2} \int\int_{-\infty}^{\infty} s(a, b) r^*(a - x, b - y) da\, db. \tag{4}$$

This function has a maximum at (x_o, y_o) that determines the parameters of the translation.

One limitation of the matched filter defined by (3) is that the output of the filter is primarily dependent on the energy of the image rather than on its spatial structures. This is why the matched filter provides a relatively poor discrimination between objects of different shapes but similar size or energy content. Furthermore, the filter output is proportional to the image auto-correlation, and the shape of the filter output around its maximum (x_o, y_o) is broad. Accurately locating this maximum is therefore difficult in the presence of noise. This problem can be solved using a phase-only matched filtering (POMF).

The transfer function of a phase-only matched filter [21] is equal to the spectral phase of the image:

$$H(u, v) = \text{Phase}(R^*(u, v)) = \exp[j(-\phi_r(u, v))], \tag{5}$$

where, $j^2 = -1$. Since the spectral phase preserves the location of objects but is insensitive to the image energy [20], [42], the application of the phase-only matched filter to a pair of identical images under the constraint of translation yields a much sharper peak than the classical matched filtering. The detection and location of the maximum is then easier, and the POMF allows a better discrimination between different objects than the matched filtering.

A further improvement of the phase-only matched filtering can be achieved by extracting and correlating the phases of both $r(x, y)$ and $s(x, y)$. This is done by defining a nonlinear filter with an output given by the inverse Fourier transform of the function:

$$Q(u, v) = \frac{S(u, v)}{|S(u, v)|} \bullet \frac{R^*(u, v)}{|R^*(u, v)|} = \exp[j(\phi_s(u, v) - \phi_r(u, v))], \tag{6}$$

where, $\phi_s(u,v)$ and $\phi_r(u,v)$ are the spectral phases of $s(x,y)$ and $r(x,y)$. In the absence of noise, this function reduces to

$$Q(u,v) = \exp[-j2\pi(ux_o + vy_o)]. \tag{7}$$

The inverse Fourier transform of (7) is a Dirac δ-function centered at (x_o, y_o), yielding an even sharper maximum than the phase-only matched filter. This technique, referred to as a symmetric phase-only matched filtering (SPOMF), can be seen as a nonlinear two step process, the first step being the extraction of the phases of the input images and the second the phase-only matched filtering [27]. Some further improvements of the symmetric phase-only matching can be achieved by preprocessing the spectral phases [22], [24], [43]–[45].

III. The Fourier–Mellin Invariant Descriptor

Consider an image $s(x,y)$ that is a rotated, scaled, and translated replica of $r(x,y)$,

$$s(x,y) = r[\sigma(x\cos\alpha + y\sin\alpha) - x_o, \\ \sigma(-x\sin\alpha + y\cos\alpha) - y_o)], \tag{8}$$

where α is the rotation angle, σ the uniform scale factor, and x_o and y_o are the translational offsets. The Fourier transforms of $s(x,y)$ and $r(x,y)$ are related by

$$S(u,v) = e^{-j\phi_s(u,v)}\sigma^{-2}|R[\sigma^{-1}(u\cos\alpha + v\sin\alpha), \\ \sigma^{-1}(-u\sin\alpha + v\cos\alpha)]|, \tag{9}$$

where $\phi_s(u,v)$ is the spectral phase of the image $s(x,y)$. This phase depends on the translation, scaling and rotation, but the spectral magnitude

$$|S(u,v)| = \sigma^{-2}|R[\sigma^{-1}(u\cos\alpha + v\sin\alpha) \\ \sigma^{-1}(-u\sin\alpha + v\cos\alpha)]|, \tag{10}$$

is translation invariant.

Equation (10) shows that a rotation of the image rotates the spectral magnitude by the same angle, and that a scaling by σ scales the spectral magnitude by σ^{-1}. Another useful property is the invariance of the spectral origin $u = v = 0$ for rotation and scaling. Rotation and scaling can be decoupled by defining the spectral magnitudes of $\mathbf{r}$ and $\mathbf{s}$ in the polar coordinates (θ, ρ),

$$r_p(\theta,\rho) = |R(\rho\cos\theta, \rho\sin\theta)| \tag{11}$$

$$s_p(\theta,\rho) = |S(\rho\cos\theta, \rho\sin\theta)|. \tag{12}$$

Note that the spectral magnitude is a periodic function of the polar angle θ [53], if the original image is real,

$$r_p(\theta \pm n\pi, \rho) = r_p(\theta,\rho); \text{ for } n = \cdots, -2, -1, 0, 1, 2, \cdots \tag{13}$$

Therefore, half of the magnitude field is sufficient to estimate the filter transfer function. Using

$$\begin{cases} \sigma^{-1}(u\cos\alpha + v\sin\alpha) & = \frac{\rho}{\sigma}\cos(\theta - \alpha) \\ \sigma^{-1}(-u\sin\alpha + v\cos\alpha) & = \frac{\rho}{\sigma}\sin(\theta - \alpha) \end{cases} \tag{14}$$

one easily checks that

$$s_p(\theta,\rho) = \sigma^{-2} r_p(\theta - \alpha, \rho/\sigma). \tag{15}$$

Hence an image rotation shifts the function $s_p(\theta,\rho)$ along the angular axis. A scaling is reduced to a scaling of the radial coordinate and to a magnification of the intensity by a constant factor σ^2. Scaling can be further reduced to a translation by using a logarithmic scale for the radial coordinate. We define

$$r_{\text{pl}}(\theta,\lambda) = r_p(\theta,\rho) \tag{16}$$

$$\text{and } s_{\text{pl}}(\theta,\lambda) = s_p(\theta,\rho) = \sigma^{-2} r_{\text{pl}}(\theta - \alpha, \lambda - \kappa) \tag{17}$$

where, $\lambda = \log(\rho)$ and $\kappa = \log(\sigma)$. In this polar-logarithmic representation, both rotation and scaling are reduced to translations, as proposed by Pratt [4] and Schalkoff [32]. By Fourier transforming the polar-logarithmic representations, (16) and (17), one obtains

$$S_{\text{pl}}(\upsilon,\varpi) = \sigma^{-2} e^{-j2\pi(\upsilon\kappa + \varpi\alpha)} R_{\text{pl}}(\upsilon,\varpi) \tag{18}$$

where rotation and scaling now appear as phase shifts. This technique decouples image rotation, scaling, and translation, and is therefore very efficient numerically. The polar-log mapping of the spectral magnitude corresponds to a physical realizations of the Fourier–Mellin transform [31]–[39], and we call the function $r_{\text{pl}}(\theta,\lambda)$ the Fourier–Mellin invariant (FMI) descriptor of the image $r(x,y)$.

Biological visual systems appear to have some similarity with this log-polar mapping. Schwartz suggests that a log-polar mapping of the visual field provides an approximation to the striate cortex topography [46]–[48], while Cavanagh hypothesized that a log-polar frequency representation may be directly computed by the striate cortex [49], [50]. Despite the controversy about the existence of the frequency representation in the retina-cortex system [51], [52], the existence of the polar-log mapping in the visual system is commonly accepted.

IV. Fourier–Mellin Invariant Matching

The FMI descriptors of a reference image and an observed image can be matched using standard techniques such as cross correlation (CC) [34], optimal matched filtering (MF) [41], POMF, and SPOMF. In this work we use the SPOMF, which yields a high SNR and a sharp correlation peak. We first describe a "core" FMI-SPOMF algorithm, and then describe its application to image registration and to pattern recognition problems.

Given a reference image $r(x,y)$ and an observed image $s(x,y)$, the output of the FMI-SPOMF is of the form:

$$Q_o(\upsilon,\varpi) = \frac{R_{\text{pl}}{}^*(\upsilon,\varpi) \bullet S_{\text{pl}}(\upsilon,\varpi)}{|R_{\text{pl}}(\upsilon,\varpi)| \bullet |S_{\text{pl}}(\upsilon,\varpi)|}. \tag{19}$$

The core FMI-SPOMF algorithm consists of the following steps

1) compute the Fourier transform $R_{\text{pl}}(\upsilon,\varpi)$ of the FMI descriptor of the reference image $r(x,y)$,
2) extract the phase $\exp[-j\phi_r(\upsilon,\varpi)]$ of $R_{\text{pl}}(\upsilon,\varpi)$,
3) compute the Fourier transform $S_{\text{pl}}(\upsilon,\varpi)$ of the FMI descriptor of the input image $s(x,y)$,
4) extract the phase $\exp[-j(\phi_s(\upsilon,\varpi)]$ of $S_{\text{pl}}(\upsilon,\varpi)$,
5) determine the output of the SPOMF,

$$Q_o(\upsilon,\varpi) = \exp[-j(\phi_s(\upsilon,\varpi) - \phi_r(\upsilon,\varpi))]$$

6) compute the inverse Fourier transform,

$$q_o(\theta, \lambda) = \mathcal{F}^{-1}\{Q_o(v, \varpi)\}.$$

7) detect the maximum of the function $q_o(\theta, \lambda)$.

In an image registration problem, the two input images are assumed to be identical and the aim is to determine the parameters of the geometric transformation relating the two images. This can be done by first executing the FMI-SPOMF core algorithm. The maximum of the filter output $q_o(\theta, \lambda)$ is then located at a certain point $\theta = \theta_{\max}, \lambda = \lambda_{\max}$. The rotation angle is then given by $\alpha = \theta_{\max}$ and the scaling factor by $\sigma = \exp(\lambda_{\max})$. Since only half of the spectrum has been used to derive the FMI descriptor (cf. (13)) the estimated rotation angle α belongs to the interval [0, 180°], whereas the real rotation may be either α or $\alpha + 180°$. The second step of the image registration algorithm determines the translation offsets, and solves the ambiguity in the value of the rotation angle: the image $s(x, y)$ is re-scaled by σ^{-1}, and two copies of the re-scaled image are re-rotated by α and $\alpha + 180°$ respectively. The spectrum of the correctly re-rotated image differs from $R(u, v)$ only by a phase caused by the translation, while the spectrum of the incorrectly rotated image does not correlate with $R(u, v)$. The correct value of the rotation angle can therefore be determined. Then, the SPOMF of the reference image $r(x, y)$ and the correctly re-rotated and re-scaled copy of $s(x, y)$ determines the translation (x_o, y_o), as explained in Section II. The image registration algorithm is summarized as follows:

1) execute the FMI-SPOMF core algorithm,
2) locate the position (α, κ) of the maximum of $q_o(\theta, \lambda)$,
3) re-scale the image $s(x, y)$ by σ^{-1} and duplicate it,
4) re-rotate the two re-scaled images by α and $\alpha + 180°$ respectively,
5) calculate the SPOMF between $r(x, y)$ and the two re-scaled and re-rotated images respectively,
6) determine which of the two copies yields the highest filter maximum,
7) locate the position of this maximum,
8) output the parameters of the geometric transformation.

The FMI-SPOMF core algorithm can also be applied to pattern recognition problems. Here, the aim is to identify among a set of reference images the image that best matches some observed image. A pattern recognition algorithm can be achieved by adding one more step to the FMI-SPOMF core algorithm:

1) Execute the FMI-SPOMF core algorithm,
2) If the maximum of the output exceeds some pre-set threshold, one assert the presence in the input image of a rotated, scaled, and translated replica of the reference image.

The FMI descriptors depend only on the magnitudes of the Fourier transforms, and do not therefore preserve the whole information present in the images. This results in the possibility of false positive detection. Consider for instance a set of images with identical spectral magnitudes but different spectral phases. These images obviously correspond to different patterns [20], [42], but their FMI descriptors are all identical. All such patterns would match the reference image equally well and would generate false positive detection. After executing the previously described pattern recognition algorithm, the false positive detection can be avoided by comparing a re-rotated and rescaled copy of the observed image to the reference images, using the SPOMF. This procedure can easily be achieved by following the registration algorithm and adding a decision step. If the maximum of the SPOMF exceeds a given threshold, the original decision of the FMI-SPOMF is confirmed. Otherwise, a false positive has been detected by the FMI-SPOMF.

V. Implementation

The FMI-SPOMF requires several direct and inverse Fourier transforms. The discrete implementation must be done with care to avoid artifacts [53] due to sampling and truncation. It is helpful to window the images before calculating the Fourier transforms. In this work, a Hanning window has been applied to the images along each coordinate [53].

The FMI descriptor of an image $r(x, y)$ is obtained by resampling the spectral magnitude of this image to polar coordinates and then resampling the radial coordinate with a logarithmic function, or by resampling the spectral magnitude in one step onto a rectangular polar-logarithmic coordinates. Here, care needs to be taken in selecting the starting point of the logarithmic resampling, since $\lim_{\rho \to 0} \ln \rho = -\infty$. Assuming that the spectral magnitude $R(u, v)$ is presented on an $N \times N$ grid with zero frequency at $(N/2, N/2)$, we used the following function to resample the spectral magnitude onto an $M \times K$ polar-log grid in one step:

$$\begin{cases} u_{mk} = \frac{N/2-1}{M-1}(M-1)^{m/(M-1)} \cos(\frac{\pi k}{K}) + \frac{N}{2} \\ v_{mk} = \frac{N/2-1}{M-1}(M-1)^{m/(M-1)} \sin(\frac{\pi k}{K}) + \frac{N}{2} \end{cases} \quad m = 0, \cdots, M-1; k = 0, \cdots, K-1 \tag{20}$$

where m is the discrete radial coordinate and k the discrete angular coordinate, and u and v are the Cartesian frequency coordinates. In order to guarantee the resampling quality, we used a 2-D linear interpolation [54]. Fig. 1(a) shows a 256 × 256 digitized photograph of a leaf. The spectral magnitude of that image is shown in Fig. 1(b) and the same spectrum is shown in Fig. 1(c) after resampling on the polar-logarithmic grid.

The dynamic range of the spectral magnitude is usually large and the values of the spectral magnitude at the two ends of the radial axis differ by several orders of magnitude. This discontinuity can also cause artifacts when Fourier transforming the FMI descriptor. To suppress such artifacts, it is necessary to window the spectral magnitude along the radial axis before the Fourier transformation. In our implementation, we have applied a Hanning window to the image spectral magnitude along the radius direction before the polar-log resampling. Fig. 1(d) shows the windowed polar-log magnitude.

The rotation angle and scaling factor can be estimated with an accuracy that depends on the sampling defined by (20). The angular coordinate of the spectral magnitude is sampled uniformly and the precision on the rotation angle is therefore uniform. However, the logarithmic distortion along

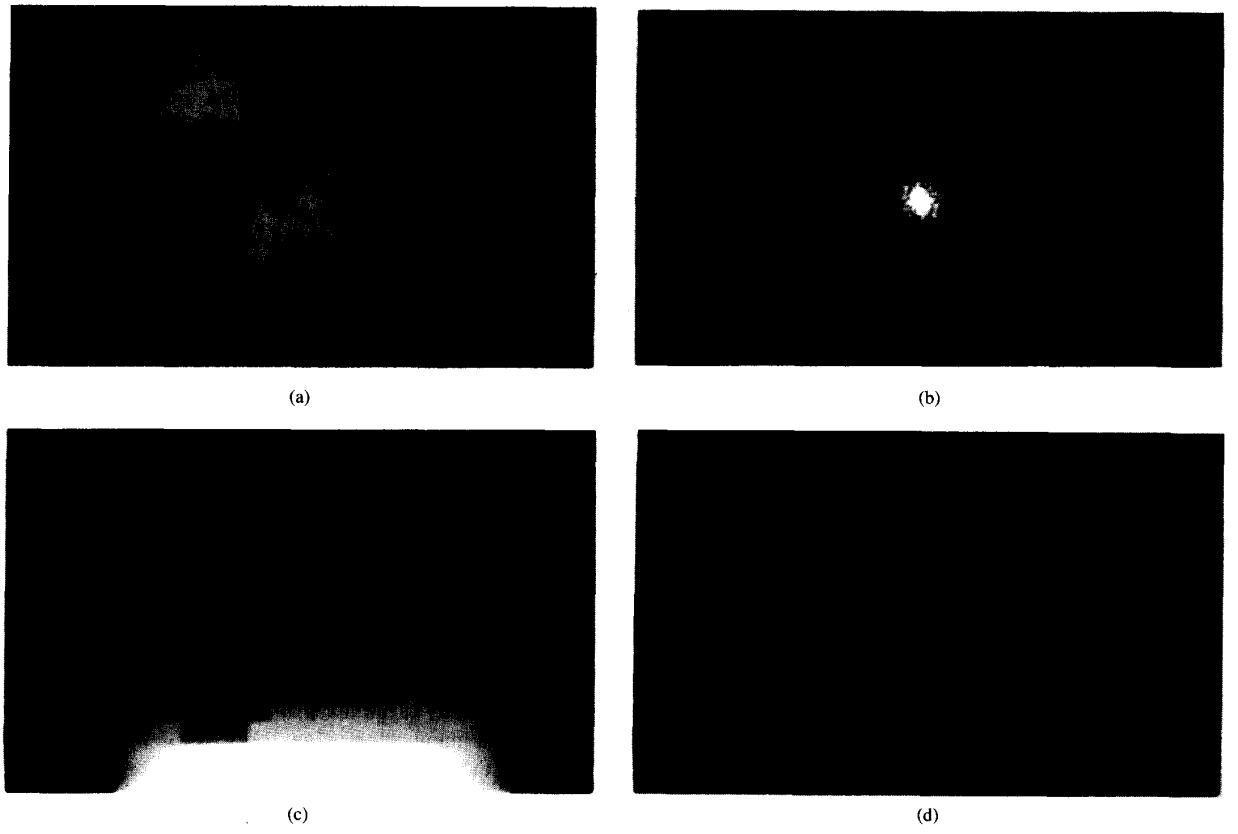

Fig. 1. (a) A leaf image with spatial dimension 256 × 256. (b) The spectral magnitude of the leaf image. (c) The polar-log resampling of the spectral magnitude (the Fourier–Mellin invariant descriptor of the leaf image), and (d) is after windowing the FMI descriptor along the radial axis.

the radial coordinate results in a non-uniform precision of the scale estimation. Indeed, suppose that the maximum of the filter output is located at a discrete radial coordinate m, with $0 \leq m < M$. Due to the folding property of the discrete Fourier transform, the corresponding scaling factor is given by:

$$\begin{cases} \sigma = (M-1)^{m/(M-1)}, & \text{for } 0 \leq m < M/2, \\ & \text{(enlargement)} \\ \sigma^{-1} = (M-1)^{(M-m)/(M-1)} & \text{for } M/2 < m \leq M \\ & \text{(shrinkage)} \end{cases} \tag{21}$$

The estimation error on s is defined as the average of the absolute difference between the real scale factor and the estimated:

$$\begin{aligned} \Delta\sigma_m &= \int_{m-\frac{1}{2}}^{m+\frac{1}{2}} dx |(M-1)^{m/(M-1)} - (M-1)^{x/(M-1)}| \\ &= \frac{M-1}{\ln(M-1)} \left[(M-1)^{1/(4(M-1))} \right. \\ &\qquad \left. - (M-1)^{-1/(4(M-1))} \right]^2 \\ &\quad \times (M-1)^{m/(M-1)}; \text{ for } 0 \leq m < M/2 \end{aligned} \tag{22}$$

and

$$\begin{aligned} \Delta(\sigma^{-1})_m = \frac{M-1}{\ln(M-1)} &\left[(M-1)^{1/(4(M-1))} \right. \\ &\left. - (M-1)^{-1/(4(M-1))} \right]^2 (M-1)^{(M-m)/(M-1)} \\ &\text{for } M/2 \leq m < M. \end{aligned} \tag{22'}$$

Thus the estimation error is proportional to σ for enlargement or to σ^{-1} for shrinkage, and the minimum is at $\sigma = 1$. For instance, if $M = N = 256$, the detectable scaling factor σ covers the range (0.0625, 16.0), and the average error on σ varies from 0.022 to 0.319, which may be better seen in Fig. 2.

The FMI-SPOMF may fail when the scale factor σ is too large or too small, because of the digitization error. The range of scale factors that can be estimated reliably should be determined experimentally. In our experiments, scale factors ranging from 50% to 200% have been determined accurately, and this range covers most practical situations.

The estimation accuracy can be improved by fitting a continuous function to the calculated discrete values of the filter output, so as to locate the maximum with a sub-pixel precision. We have fitted a triangular function along the angular and radial coordinates respectively.

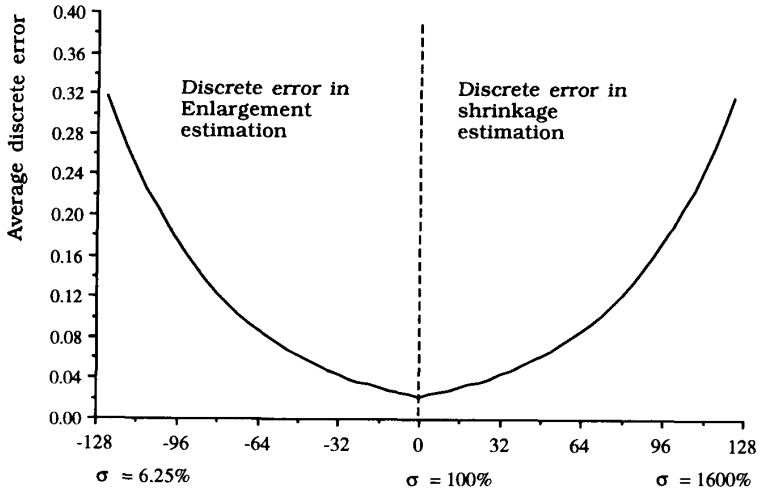

Fig. 2. The average estimation error of the scale factor.

VI. Performance Evaluation

To evaluate the performance of the FMI-SPOMF algorithm, we define three quality figures: the output signal-to-noise ratio, the sharpness of the estimation peak in the matching field, and the percent discrimination.

The output signal-to-noise ratio is defined as the ratio of the absolute signal value to the average background noise:

$$\text{SNR} = \frac{|C_{\max} - M|}{D} \tag{23}$$

where $C_{\max}$ is the maximum of the filter output and M and D are the output mean and standard deviation respectively, in the region excluding the maximum.

The sharpness of the output peak is characterized by the full area at half maximum (FAHM), namely the area of the (x, y) plane where the filter output exceeds one half the maximum value $C_{\max}$.

The percent discrimination (PD) is a measure of the similarity between the reference image and the input image:

$$\text{PD} = \frac{2[C_{\text{sr}}]_{\max}}{[C_{\text{ss}}]_{\max} + [C_{\text{rr}}]_{\max})} \bullet 100\%, \tag{24}$$

where, $[C_{\text{ss}}]_{\max}$, $[C_{\text{rr}}]_{\max}$, and $[C_{\text{sr}}]_{\max}$ are the maxima of the filter outputs when matching the reference image $s(x, y)$ to itself, the input image $r(x, y)$ to itself, and the reference image to the input image respectively. The percent discrimination is a relative measure, which can be useful to compare one image to several references.

Using above measures, the FMI-SPOMF has been compared with the matched filtering and with the phase-only matched filtering. In addition, the performance of a magnitude-only cross correlation has also been investigated. The magnitude-only cross correlation is the correlation between the spectral magnitudes of the reference image and the input image.

Using Fig. 1(a) as both the reference and the observed images, the output of the matched filtering, the phase-only matched filtering, the symmetric phase-only matched filtering, and the magnitude-only cross correlation are shown in Fig. 3(a), (b), (c), and (d) respectively. The symmetric phase-only matched filtering yields the sharpest peak and should therefore also be applied to match the FMI descriptors. On the other hand, the output of the magnitude-only cross correlation which is similar to the method used in [8], [34], [35] to register medical images is quite flat, resulting in unreliable localization of the maximum. Fig. 4(a) and (b) show the filter output obtained by applying to the FMI descriptors of the images the phase-only matched filtering and the symmetric phase-only matched filtering respectively. In both cases, the filter has an extremely sharp peak; indeed, with the limited pixel resolution (8 bits), the standard deviation of the FMI-SPOMF is zero. These results are summarized in Table I.

TABLE I
Performances of Different Matching Techniques for a Noise-Free Input Image

Filter output	MF	POMF	SPOMF	MOCC	FMI-POMF	FMI-SPOMF
SNR	4.32	50.07	$\infty*$	3.43	128.87	$\infty*$
FAHM	5323	5	1	14393	1	1

MF: matched filtering; POMF: phase-only matched filtering; SPOMF: symmetric phase-only matched filtering; MOCC: magnitude-only cross correlation.

To investigate the robustness of the FMI matched filtering, we have added white noise to the leaf image of Fig. 1(a) with SNR = 3.33. The shapes of all filtering outputs are similar to those achieved in noise free condition, but with lower output SNR's. The SNR's and FAHM's are listed in Table II. All results indicate that the FMI matched filtering is comparable with the phase-only matched filtering when dealing with image translations.

In the presence of rotation and scaling, the above techniques cannot be used except the FMI matching. The output of the FMI-SPOMF applied to the leaf image in Fig. 1(a) and a replica of the image after 100° of rotation and 90% of scaling yields a dominant peak at (114, 251) with the output SNR

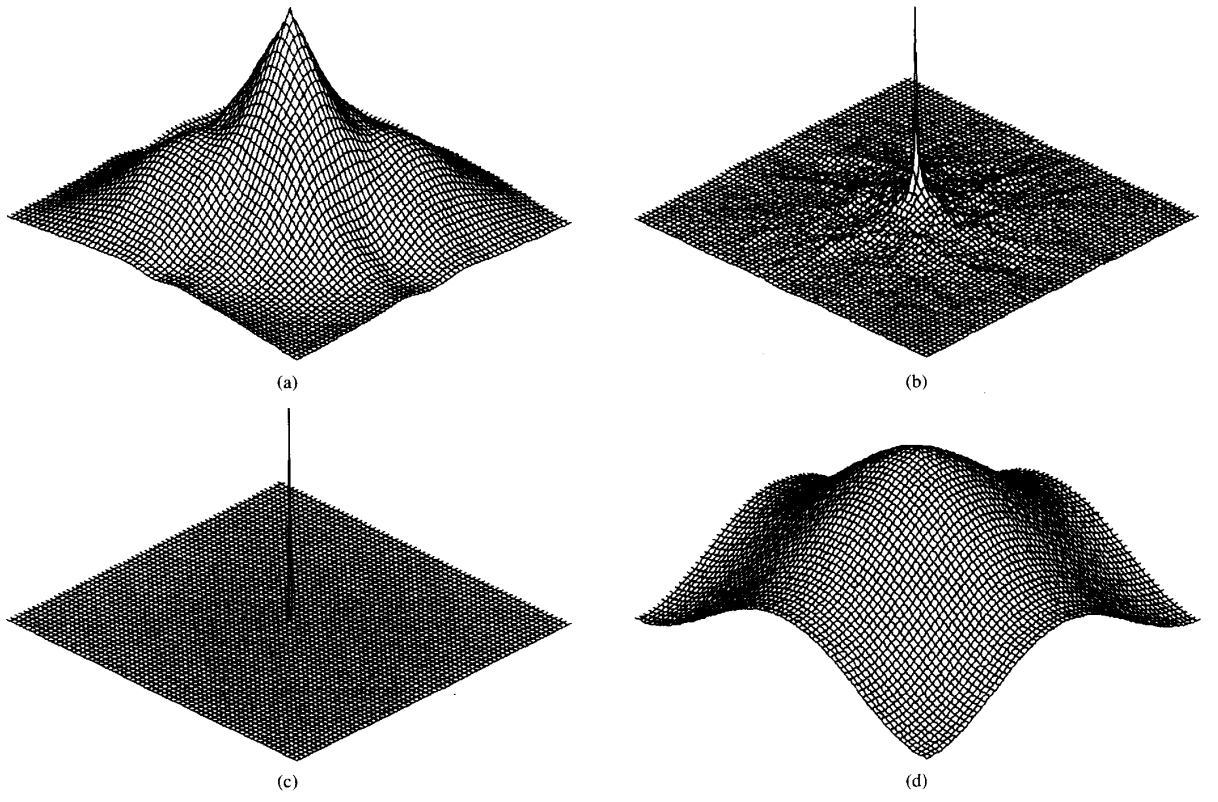

Fig. 3. (a) The output of the matched filtering applied to the leaf image, Fig. 1(a), as both the reference and the image to be matched. (b) The POMF. (c) The SPOMF. (d) The magnitude-only cross-correlation.

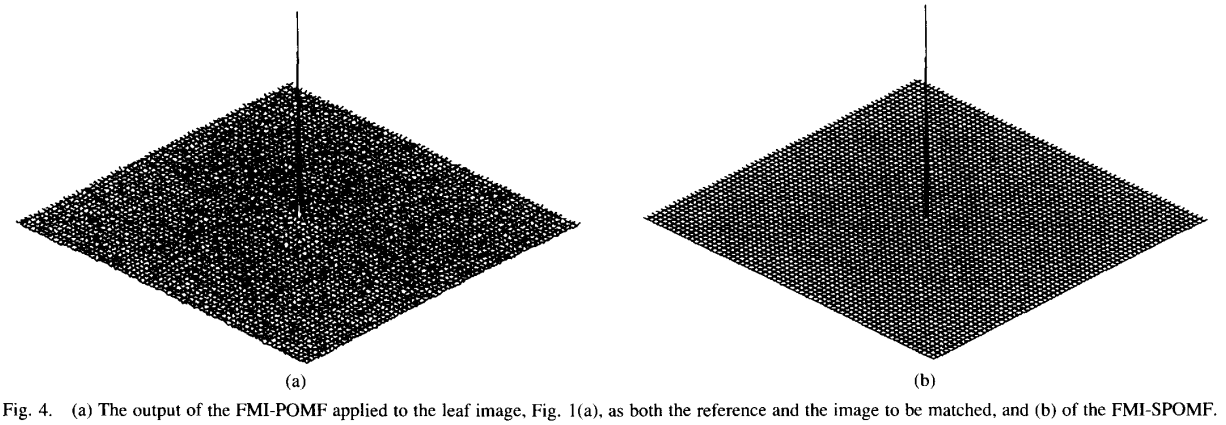

Fig. 4. (a) The output of the FMI-POMF applied to the leaf image, Fig. 1(a), as both the reference and the image to be matched, and (b) of the FMI-SPOMF.

TABLE II
PERFORMANCES OF DIFFERENT MATCHING TECHNIQUES FOR AN INPUT SNR OF 3.33

Filter output	MF	POMF	SPOMF	MOCC	FMI-POMF	FMI-SPOMF
SNR	3.67	34.96	51.55	3.28	39.23	52.10
FAHM	5323	5	1	15113	1	1

= 48.0, corresponding to the estimated rotation angle 99.84° and scale factor 89.7%. The precision can be further improved by following the sub-pixel estimation proposed in Section V. In our test, the sub-pixel estimation moves the maximum to (113.7, 251.2) and the corresponding rotation angle and scale factor are 100.06° and 90.08%.

After adding white noise (SNR = 3.33) to the rotated and scaled replica of the leaf image, Fig. 5(a), the FMI-SPOMF output is shown in Fig. 5(b) with the maximum located at (114, 251) and the output SNR = 19.1. Fig. 6(a) is another replica of the leaf image after 30° of rotation and 200% of scaling change. Although part of the object has been truncated, the FMI-SPOMF still locates the correlation peak correctly, as

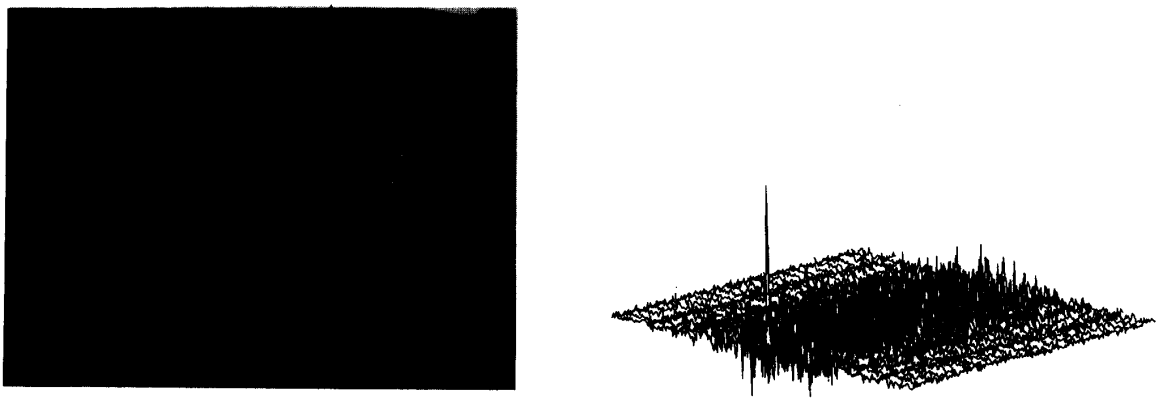

(a) (b)

Fig. 5. The matching of the rotated and scaled version of the leaf image using the FMI-SPOMF. (a) A noise corrupted version of the rotated and scaled leaf image with rotation angle 100° and scale rate 90% and with SNR = 3.33. (b) is the output of the FMI-SPOMF applied to (a) and Fig. 1(a). The peak, with output SNR = 19.01 and FAHM = 3 pixels, is located at (114, 251), corresponding to rotation angle 99.84° and scale rate 89.7%.

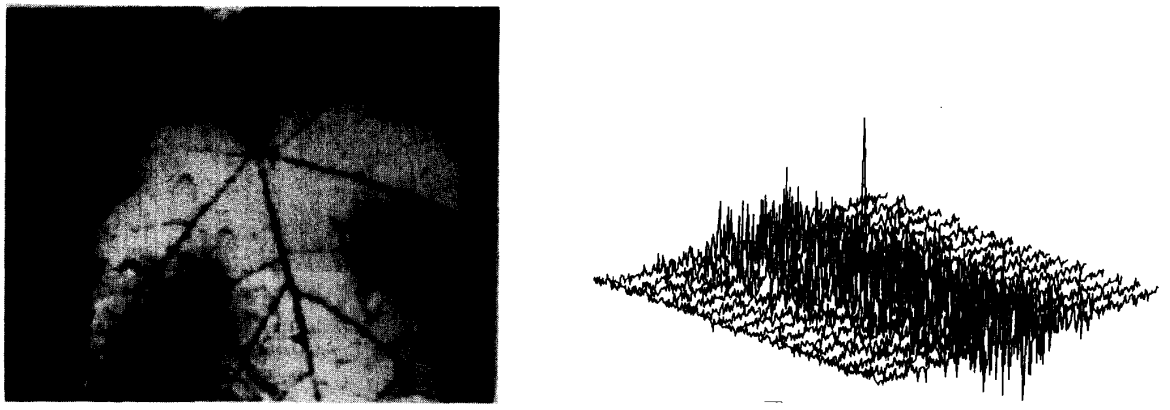

(a) (b)

Fig. 6. (a) A rotated and enlarged version of the leaf image in Fig. 1(a), with rotation angle 30° and scale rate 200%, where the image is partially occluded. (b) The output of the FMI-SPOMF applied to (a) and Fig. 1(a). The peak corresponds to the rotation and scaling with output SNR = 10.58 and FAHM = 4 pixels.

shown in Fig. 6(b) with output SNR = 10.6 and peak location at (213, 32) corresponding to the rotation and scaling (30.2°, 200.5%).

VII. Applications

This section describes some applications of the FMI-SPOMF to medical image registration, remote sensing image matching, fingerprint recognition, and multi-object identification.

A. Registration of Medical Images

In clinical diagnosis, as well as in radiotherapy planning and evaluation, several images of one patient, obtained using different imaging modalities or at different times, need to be compared. This comparison is effective only when these images are correctly aligned (registered) [55]–[58].

Fig. 7(a) and (b) show two slices through three-dimensional magnetic resonance (MR) images of a patient, taken with two different pulse sequences that yield images reflecting primarily the value of the transverse relaxation time T2 (a measure for the rate of energy redistribution among hydrogen spins) and of the longitudinal relaxation time T1 (the energy transfer rate between the hydrogen spins and the surrounding tissue). The two 3D images have been registered as follows, assuming for simplicity that the slices in the two images are parallel. One slice of interest in the T2 image volume was selected as reference image. Using the FMI-SPOMF, this reference image was then compared to all slices of the T1 image volume. The T1 slice best matching the reference was used to estimate the transformation parameters, as explained in Section V. The output of the FMI-SPOMF applied to the best matched T2 and T1 slices is shown in Fig. 8(a), with output SNR = 17.59 and FAHM = 3. The peak corresponds to the rotation angle 6° and scale factor 100%. After reversely rotating the T1 image, we applied the SPOMF to these two images to determine the translation. The SPOMF output is shown in Fig. 8(b) and the peak corresponds to the translation (5, −4) pixels. In Fig. 7(c), a region-of-interest corresponding to the cortex has

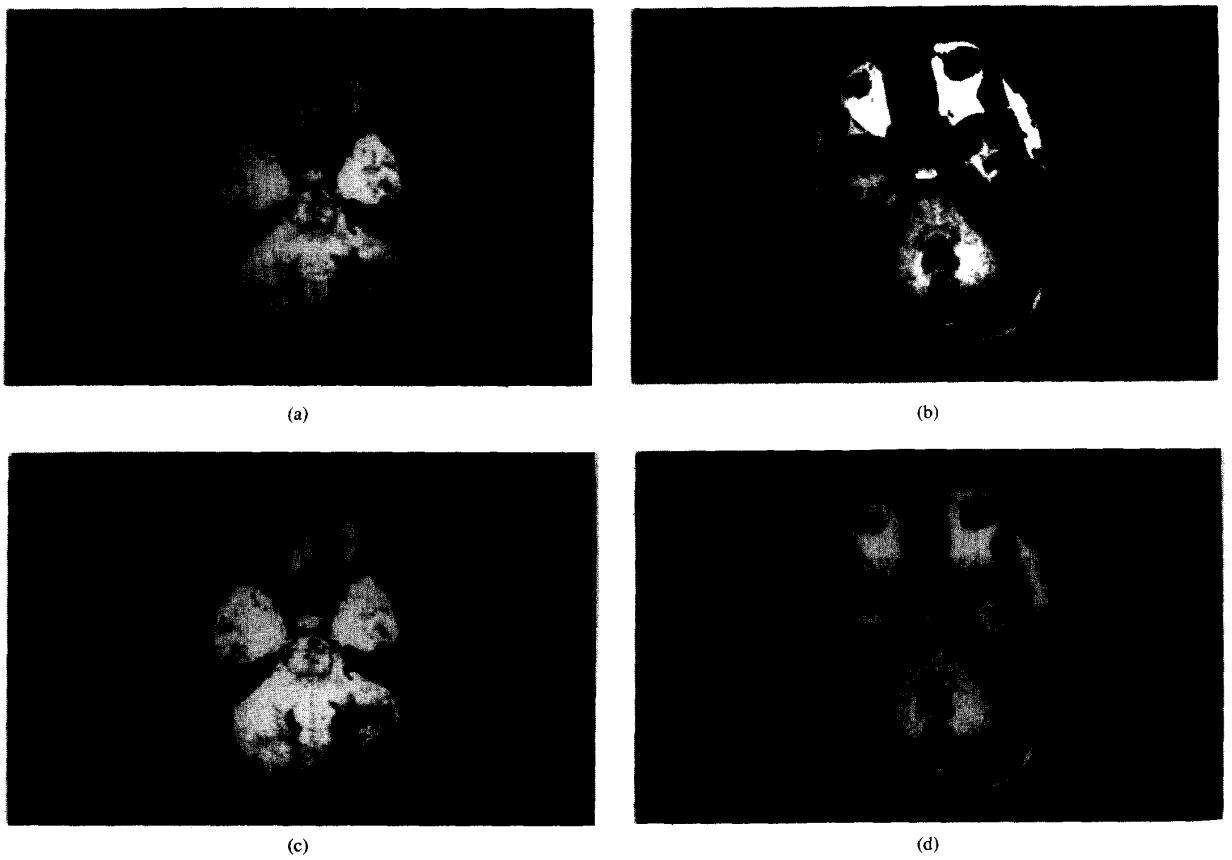

Fig. 7. (a) A slice from an MRT2 weighted volume image of a patient with slice dimension 256 × 256. (b) The slice of the MR T1 weighted image of the same patient, which best matches the T2 slice in (a) with the FMI-SPOMF. (c) The cortex in the T2 slice has been selected as the region of interests. The same anatomical region in the T1 slice is automatically located after registration.

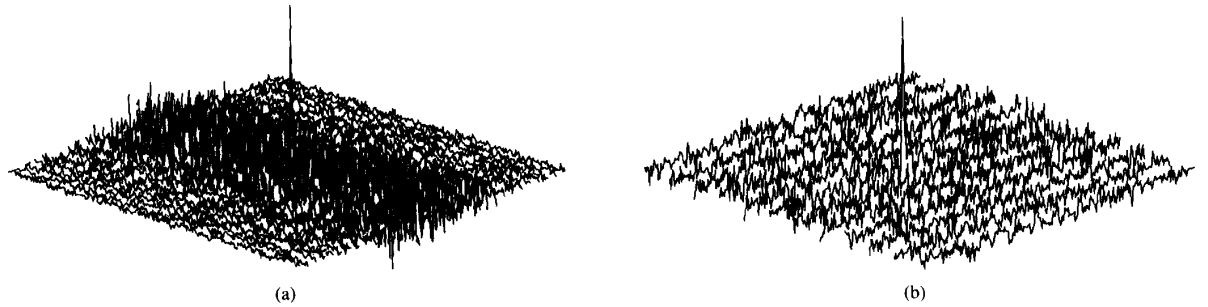

Fig. 8. The output of the FMI-SPOMF applied to the two MR slices in Fig. 8(a) and (b). The peak corresponds to rotation 6° and scale rate 100%. (b) The output of the SPOMF applied to the two MR slices, after the T1 slice was rotated by −6°. The peak corresponds to the translational offsets (−5, 4).

been delineated manually in the T2 image and this contour has been superimposed onto the T1 image, demonstrating the accuracy of the registration. The result is shown in Fig. 7(d).

B. Remote Sensing Image Matching

Automatic data processing of remote sensing images involves the evaluation, inventory, and identification of environmental structures. Chronological observations, sensor-to-sensor comparisons, and synthesis of color composite images all require the registration of different images of the same scene [59]–[61].

Fig. 9(a) and (b) show two SPOT images of the same scene taken at different dates. Since the altitude of the sensing platform is much larger than the topographic height variations, the photographs are approximately parallel projections and the perspective projection distortions between the images can be ignored. The geometric transform relating the two images can therefore be determined using our new technique. The output

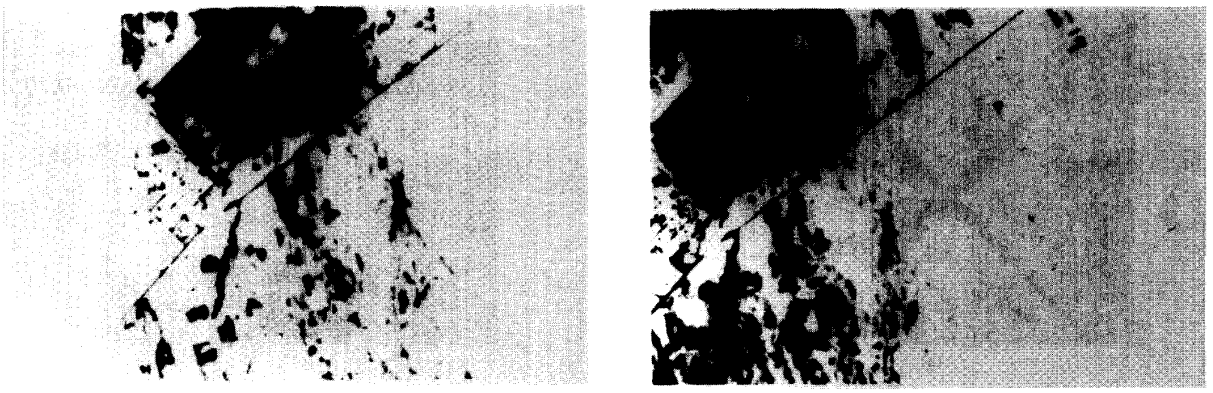

(a) (b)

Fig. 9. (a) A SPOT remote sensing image taken on Feb. 24, 1986. (b) Another SPOT remote sensing image taken from the same terrain as in (a), but on Feb. 25, 1986. Owing to the uncontrollable natural luminance, the intensities of the two images are not exactly the same.

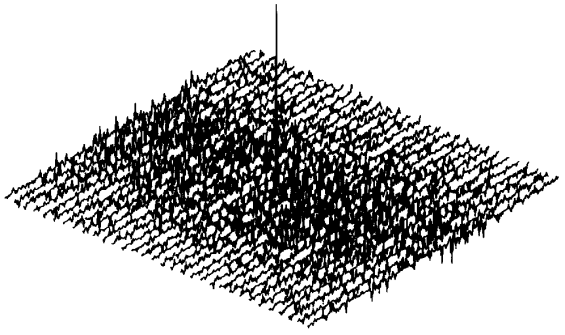

Fig. 10. The output of the FMI-SPOMF applied to the two remote sensing images, Fig. 9(a) and (b), to estimate the rotation and scaling difference. The peak corresponds to rotation angle 7° and scaling rate 100%.

of the FMI-SPOMF filtering is shown in Fig. 10 with an output SNR = 37.33 and a FAHM = 4. The corresponding rotation angle is 7° and the scale factor 100%. After re-rotating the image in Fig. 9(b), the image translation is estimated using the SPOMF. The output of the SPOMF applied to the two images has a maximum corresponding to a translation (−12, 1) with the ground distance (12 × 200 m, 200 m).

C. Fingerprint Recognition

Fingerprint recognition, one of the reliable method for personal identification, is based on the identification and matching of fingerprint minutiae, which are irregularities such as ridge endings and joinings whose types and locations are unique for every individual. In a fingerprint recognition system, the observed print is first segmented and binarized. Then, all minutiae are identified and their locations recorded as a graph in a 2-D plane. Matching is achieved by determining the similarity between this graph and the graphs in the reference fingerprint databank. The most difficult step in this system is the correct identification of the minutiae [62]–[66].

A variety of efficient and robust fingerprint identification systems have been based on the use of optical correlation. Unfortunately, optical correlation can identify two prints only if their orientations are almost identical [67].

TABLE III
THE PERCENT DISCRIMINATIONS OF THE FINGERPRINT MATCHING BY THE FMI-SPOMF ALGORITHM*

Fingerprint	Print (a)	Print (b)	Print (c)	Print (d)
PD (%)	54.97	38.75	34.48	41.78

*The new print and print (a) were originally taken from the same finger.

The FMI-SPOMF can be used to recognize fingerprints even when the orientations are not identical. We have collected as references the prints of four different fingers. A new print was then taken from one of the four fingers, and compared to the four references using FMI-SPOMF. As shown in Table III, the correct print yields the highest maximum, although the difference with the other, mismatched, prints is less than a factor of two. This result is nevertheless significant, because the usual cross-correlation method, which we applied in comparison, did not yield any correct matching.

These results are inferior to those observed with the other applications presented in this paper, indicating that the FMI-SPOMF is not optimal for fingerprint recognition. It should be noted, however, that this experiment was based on real data without any preprocessing and with a rather poor quality of the prints. The discrimination power could probably be improved by appropriate image enhancement.

D. Multi-Object Identification

Robot vision requires the analysis and identification of relatively simple objects that may in some cases overlap in the vision field. Most vision systems identify these objects by matching their contours. Correct segmentation of the object contours requires some assumptions, which are not always satisfied in practice. Indeed, many demonstrations of the vision systems have used ideal images obtained under tight control or using models synthesizes by computer [68]–[70].

We have tested the efficiency of the FMI-SPOMF for a simple multi-object identification task. Fig. 11(a) is a two object view. The task is to detect and locate the key, Fig. 11(b). The FMI-SPOMF output is shown in Fig. 12(a), where the high peak indicates that the key is present in the scene. Fig. 12(b)

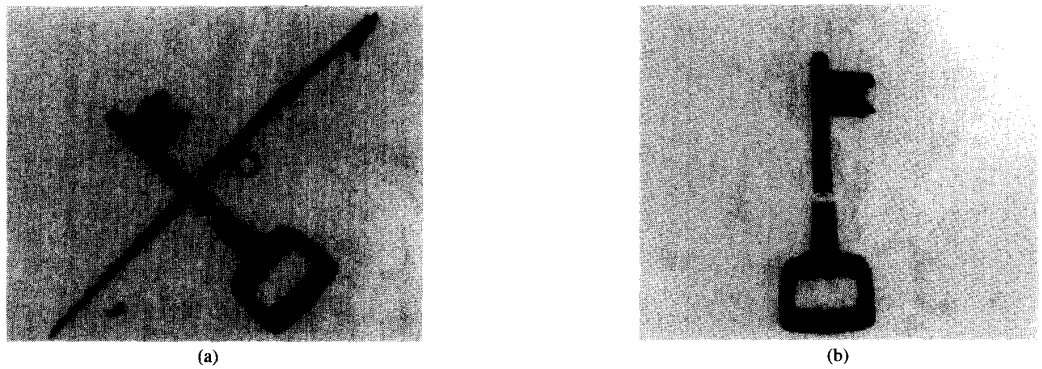

(a) (b)

Fig. 11. (a) A key-knife image. (b) A key template to be detected from image (a).

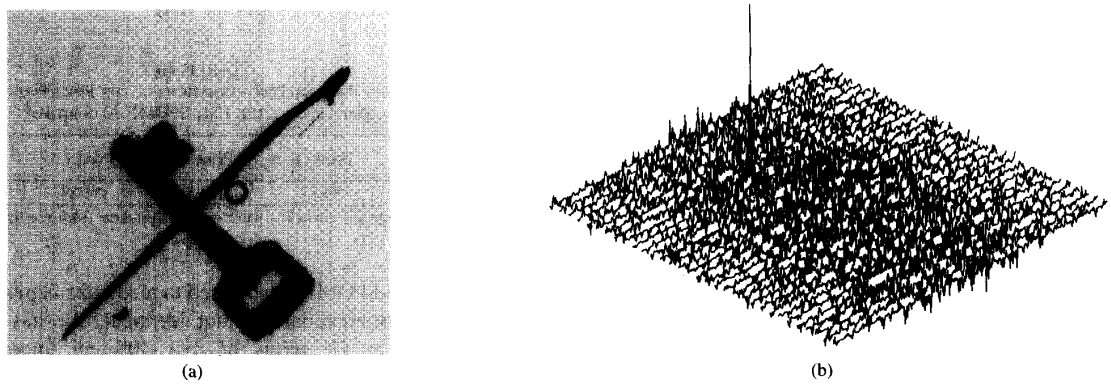

(a) (b)

Fig. 12. (a) The output of the FMI-SPOMF applied to Fig. 11 (a) and (b), where the peak corresponds to the rotation angle 44° and scale rate 100%. (b) The key has been detected and located in the key-knife image.

shows the delineated detected key. The main advantage of the FMI-SPOMF over contour matching techniques is the absence of preprocessing, such as segmentation, which results in a much more efficient implementation.

VIII. Conclusion

The Fourier–Mellin invariant symmetric phase-only matched filtering (FMI-SPOMF) is a general, robust, and efficient image matching technique. The performance of the FMI-SPOMF are identical to the usual symmetric phase-only matched filtering when the images to be matched are related by a translation only. The significant advantage of the FMI-SPOMF is its ability to match rotated and scaled images, even in the presence of noise and with partial occlusion of the object in one image. This robustness is due to the sharpness of the maximum of the filter output, a sharpness that also ensures a good discriminating power between similar images. The FMI-SPOMF can be applied to image recognition and image registration, as was demonstrated by the various applications presented in this paper.

Currently, the method has been tested only with images without background, or with images where the object and the background were rotated and scaled simultaneously. Further investigation is required to evaluate the method when the geometric changes of the object and of the background do not coincide, or when the background is not identical in the two images. Further work will also involve the optimization of the transfer function of the FMI-SPOMF when prior knowledge of the statistical distribution of the object, noise, and background is available. Finally, an open problem is the extension of the method to three-dimensional problems.

Acknowledgment

The authors are grateful to their colleague S. Kuijk for his help with computer work. The first author would like to express sincerely his gratitude to Prof. M. H. Jonckheer for his continuous encouragement and support. Thanks also go to the reviewers of this paper, especially the first reviewer who has not only raised several critical remarks but also kindly provided a long list of references. The authors would also like to express their gratitude to the Associate Editor, Prof. J. G. Daugman, who has also raised several important comments and provided several constructive suggestions. Part of the work in this paper was performed with the ANALYZE image analysis program. The authors are grateful to the Biodynamics Research Unit, Mayo Foundation, for providing the ANALYZE software. M. Defrise is a research associate with the National Fund for Scientific Research (Belgium).

REFERENCES

[1] D. I. Barnea and H. F. Silverman, "A class of algorithms for fast image registration," *IEEE Trans. Comput.*, vol. 21, no. 2, pp. 179–186, 1972.

[2] G. J. Vanderburg and A. Rosenfeld, "Two-stage template matching," *IEEE Trans. Comput.*, vol. 26, pp. 384–393, 1977.

[3] M. Svedlow, C. D. McGlem, and P. E. Anuta, "Image registration: Similarity measure and processing method comparisons," *IEEE Trans. Aerosp. Electron. Syst.*, vol. 14, no. 1, pp. 141–149, 1978.

[4] W. K. Pratt, *Digital Image Processing*.New York: John Wiley & Sons, 1978, pp. 526–566.

[5] A. Goshtasby, "Template matching in rotated images," *IEEE Trans. Pattern Anal. Machine Intell.*, vol. 7, no. 3, pp. 338–344, 1985.

[6] E. Peli, R. A. Angliere, and G. T. Timberlake, "Feature-based registration of retinal images," *IEEE Trans. Med. Imag.*, vol. 6, no. 3, pp. 272–278, 1987.

[7] S. Mitra, B. S. Nutter, T. F. Krile, and R. H. Brown, "Automatic method for fundus image registration and analysis," *Applied Optics*, vol. 27, no. 6, pp. 1107–1112, 1988.

[8] J. Segman, "Fourier cross correlation and invariant transformations for an optimal recognition of functions deformed by affine groups," *J. Opt. Soc. Am. A.*, vol. 9, no. 6, pp. 895–902, 1992.

[9] A. Venot and V. Leclerc, "Automated correlation of patient motion and gray value prior to subtraction in digitized angiography," *IEEE Trans. Med. Imag.*, vol. 3, no. 4, pp. 179–186, 1984.

[10] A. Venot, J. C. Liehn, J. F. Lebruchec, and J. C. Roucayrol, "Automated comparison of scintigraphic images," *J. Nucl. Med.*, vol. 27, pp. 1337–1342, 1986.

[11] M. K. Hu, "Visual pattern recognition by moment invariants," *IRE Trans. Information Theory*, vol. 8, pp. 179–187, 1962.

[12] Y. S. Abu-Mostafa and D. Psaltis, "Recognition aspects of moment invariants," *IEEE Trans. Pattern Anal. Machine Intell.*, vol. 6, no. 6, pp. 698–706, 1984.

[13] M. R. Teague, "Image analysis via the general theory of moments," *J. Opt. Soc. Am.*, vol. 70, no. 8, pp. 920–930, 1980.

[14] C. H. Teh and R. T. Chin, "On image analysis by the methods of moments," *IEEE Trans. Pattern Anal. Machine Intell.*, vol. 10, no. 4, pp. 496–513, 1988.

[15] M. O. Freeman and B. E. A. Salch, "Moment invariants in the space and frequency domains," *J. Opt. Soc. Am. A.*, vol. 5, no. 7, pp. 1073–1084, 1988.

[16] J. Altmann and H. J. P. Reitbock, "A fast correlation method for scale- and translation-invariant pattern recognition," *IEEE Trans. Pattern Anal. Machine Intell.*, vol. 6, no. 1, pp. 46–57, 1984.

[17] Z. Y. Sheng, C. Lejeune, and H. H. Arsenault, "Frequency-domain Fourier–Mellin descriptors for invariant pattern recognition," *Optical Engineering*, vol. 27, no. 5, pp. 354–357, 1988.

[18] S. S. Reddi, "Radial and angular moment invariants for image identification," *IEEE Trans. Pattern Anal. Machine Intell.*, vol. 3, no. 2, pp. 240–242, 1981.

[19] H. Rusinck, A. Levy, and M. E. Noz, "Performance of two methods for registering PET and MR brain scans," *Conf. Record 1991 IEEE Nuclear Science Symp. Med. Imag. Conf.*, vol. 3, pp. 2159–2162, 1991.

[20] A. V. Oppenheim and J. S. Lim, "The importance of phase in signals," *IEEE Proc.*, vol. 69, no. 5, pp. 529–541, 1981.

[21] J. L. Horner and P. D. Gianino, "Phase-only matched filtering," *Applied Optics*, vol. 23, no. 6, pp. 812–816, 1984.

[22] B. V. K. V. Kumar and Z. Bahri, "Efficient algorithm for designing a ternary valued filter yielding maximum signal to noise ratio," *Applied Optics*, vol. 28, no. 10, pp. 1919–1925, 1989.

[23] B. Javidi and J. Wang, "Binary nonlinear joint transform correlation with median and subset median thresholding," *Applied Optics*, vol. 30, no. 8, pp. 967–976, 1991.

[24] O. K. Ersoy and M. Zeng, "Nonlinear matched filtering," *J. Opt. Soc. Am. A.*, vol. 6, no. 5, pp. 636–648, 1989.

[25] T. Kotzer, J. Rosen, and J. Shamir, "Phase extraction pattern recognition," *Applied Optics*, vol. 31, no. 8, pp. 1126–1137, 1992.

[26] B. V. K. V. Kumar and E. Pochapsky, "Signal-to-noise ratio considerations in modified matched spatial filters," *J. Opt. Soc. Am. A.*, vol. 3, no. 6, pp. 777–786, 1986.

[27] E. De Castro and C. Morandi, "Registration of translated and rotated images using finite Fourier transforms," *IEEE Trans. Pattern Anal. Machine Intell.*, vol. 9, no. 5, pp. 700–703, 1987.

[28] D. J. Lee, F. Krile, and S. Mitra, "Power cepstrum and spectrum techniques applied to image registration," *Applied Optics*, vol. 27, no. 6, pp. 1099–1106, 1988.

[29] Y. N. Hsu, H. H. Arsenault, and G. April, "Rotation-invariant digital pattern recognition using circular harmonic expansion," *Applied Optics*, vol. 21, no. 22, pp. 4012–4015, 1982.

[30] Y. N. Hsu and H. H. Arsenault, "Optical pattern recognition using circular harmonic expansion," *Applied Optics*, vol. 21, no. 22, pp. 4016–4019, 1982.

[31] J. K. Brousil and D. R. Smith, "A threshold logic network for shape invariance," *IEEE Trans. Comput.*, vol. 16, pp. 818–828, 1967.

[32] R. J. Schalkoff, *Digital Image Processing and Computer Vision*. New York: John Wiley & Sons, 1989, pp. 279–286.

[33] Y. Sheng and H. H. Arsenault, "Experiments on pattern recognition using invariant Fourier–Mellin descriptors," *J. Opt. Soc. Am. A.*, vol. 3, no. 6, pp. 771–776, 1986.

[34] A. Apicella, J. S. Kippenhan, and J. H. Nagel, "Fast multi-modality image matching," in *Medical Imaging III: Image Processing*, SPIE vol. 1092, pp. 252–263, 1989.

[35] D. Casasent and D. Psaltis, "Position, rotation and scale-invariant optical correlation," *Applied Optics*, vol. 15, pp. 1793–1799, 1976.

[36] ——, New optical transforms for pattern recognition," *Proc. IEEE*, vol. 65, pp. 77–84, 1977.

[37] ——, "Positional, rotational and scale invariant optical correlation method and apparatus," *U.S. Patent 4*, 084, 255, 1978.

[38] C. Braccini, G. Gambardella, and A. Grattarola, "Shift-variant image processing for scale-invariant recognition," *Proc. SPIE*, vol. 397, pp. 318–325, 1983.

[39] L. Massone, G. Sandini, and V. Tagliasco, "'Form-invariant' topological mapping strategy for 2D shape recognition," *CVGIP*, vol. 30, pp. 169–188, 1985.

[40] A. Vanderlugt, "Signal detection by complex spatial filtering," *IEEE Trans. Inf. Theory*, vol. 10, pp. 130–145, 1969.

[41] A. D. Whalen, *Detection of Signals in Noise*. Academic Press, 1971, pp. 167–178.

[42] Q. S. Chen, "Image Registration and its Applications in Medical Imaging," Ph.D. Thesis, Free University Brussels (VUB), 1993.

[43] J. H. Horver and P. D. Gianino, "Pattern recognition with binary phase-only filters," *Appl. Opt.*, vol. 24, pp. 609–611, 1985.

[44] D. L. Flannery, J. S. Loomis, and M. E. Milkovich, "Transform-ratio ternary phase-amplitude filter formulation for improved correlation discrimination," *Appl. Opt.*, vol. 27, no. 19, pp. 4079–4083, 1988.

[45] Z. Q. Wang, W. A. Gillespie, C. M. Cartwright, *et al.*, "Optical pattern recognition using a synthetic discriminant amplitude-compensated matched filter," *Appl. Opt.*, vol. 32, no. 2, pp. 184–189, 1993.

[46] E. L. Schwartz, "Spatial mapping in primate sensory projection: Analytic structure and relevance to perception," *Biological Cybernetics*, vol. 25, pp. 181–194, 1977.

[47] ——, "Computational anatomy and functional architecture of striate cortex: A spatial mapping approach to perceptual coding," *Vision Res.*, vol. 20, pp. 645–669, 1980.

[48] ——, "Cortical anatomy and spatial frequency analysis," *Perception*, vol. 10, pp. 455–468, 1981.

[49] P. Cavanagh, "Size and position invariance in the visual system," *Perception*, vol. 7, pp. 167–177, 1978.

[50] ——, "Functional size inrariant is not provided by the cortical magnification factor," *Vision Res.*, vol. 22, pp. 1409–1412, 1982.

[51] ——, "Size invariance: Reply to Schwartz," *Perception*, vol. 10, pp. 491–499, 1981.

[52] E. L. Schwartz, "Cortical mapping and perceptional invariance: A replay to Cavanagh," *Vision Research*, vol. 23, pp. 831–835, 1983.

[53] R. N. Bracewell, *The Fourier Transform and its Applications*, New York: McGraw-Hill, 1986.

[54] A. Rosenfeld and A. C. Kak, *Digital Picture Processing*. New York: Academic Press, p. 177, 1976.

[55] M. Singh and W. Frey, T. Shibata, G. C. Huth, and N. E. Telfer, "A digital technique for accurate change detection in nuclear medical images—with application to myocardial perfusion studies using Thallium-201," *IEEE Trans. Nucl. Science*, vol. 26, no. 1, pp. 565–573, 1979.

[56] P. Gerlot and Y. Bizais, "Image registration: A review and a strategy for medical applications," in *Information Processing in Medical Imaging*, C. N. de. Graaf and M. A. Viergever, Eds. New York: Plenum Press, 1987, pp. 81–89.

[57] C. C. Meltzer, R. N. Bryan, , H. H. Holcomb, A. N. Kimball, H. S. Mayberg, B. Sadzot, J. P. Leal, H. N. Wagner, and J. J. Frost, "Anatomical localization for PET using MR imaging," *J. Computer Assisted Tomography*, vol. 14, no. 3, pp. 418–426, 1990.

[58] B. L. Holman, R. E. Zimmerman, K. A. Johnson, P. A. Carvalho, R. B. Schwartz, J. C. Loeffler, E. Alexander, C. A. Pelizzari, and C. T. Chen, "Computer-assisted superimposition of magnetic resonance and high-resolution Technetium-99m-HMPAO and Thallium-201 SPECT images of brain," *J. Nucl. Medicine*, vol. 32, 8, pp. 1478–1484, 1991.

[59] G. Nagy, "Digital image-processing activities in remote sensing for earth resources," *Proc. IEEE*, vol. 60, no. 10, pp. 1177–1200, 1972.

[60] R. M. Haralick, "Automatic remote sensor image processing," in *Digital Picture Analysis*.A. Rosenfeld, Ed. New York: Springer-Verlag, 1976, pp. 5–66.
[61] D. A. Landgrebe, "Analysis technology for land remote sensing," *Proc. IEEE*, vol. 69, no. 5, 1981, pp. 628–642.
[62] D. H. McMahon, G. L. Johnson, S. L. Teeter, C. G. Whitney, "A hybrid optical computer processing technique for fingerprint identification," *IEEE Trans. Comput.*, vol. 24, no. 4, 1975, pp. 358–369.
[63] C. V. K. Rao, "On fingerprint pattern recognition," *Pattern Recognition*, vol. 10, pp. 15–18, 1978.
[64] D. K. Isenor and S. G. Zaky, "Fingerprint identification using graph matching," *Pattern Recognition*, vol. 19, no. 2, pp. 113–122, 1986.
[65] B. M. Mehtre, N. N. Murthy, and S. Kapoor, "Segmentation of fingerprint images using the directional image," *Pattern Recognition*, vol. 20, no. 4, pp. 429–435, 1987.
[66] L. O. Gorman and J. V. Nickerson, "An approach to fingerprint filter design," *Pattern Recognition*, vol. 22, no. 1, pp. 29–38, 1989.
[67] F. T. Gamble, L. M. Frye, and D. R. Grieser, "Real-time fingerprint verification system," *Applied Optics*, vol. 31, no. 5, pp. 652–655, 1992.
[68] B. Bhanu and O. D. Faugeras, "Shape matching of two-dimensional objects," *IEEE Trans. Pattern Anal. Machine Intell.*, vol. 6, no. 2, pp. 137–155, 1984.
[69] D. Vernon, "Two-dimensional object recognition using partial contours," *Image and Vision Computing*, vol. 5, no. 1, pp. 21–27, 1987.
[70] H. C. Liu and M. D. Srinath, "Partial shape classification using contour matching in distance transformation," *IEEE Trans. Pattern Anal. Machine Intell.*, vol. 12, no. 11, 1990, pp. 1072–1079.

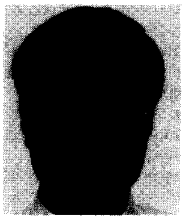

Q. S. Chen received the Bachelor of Electronic Engineering degree and the Master in Biomedical Engineering degree from Xian Jiao-tong University, China, in 1982 and 1984 respectively. From 1984 to 1988, he worked as a member of the teaching staff of Xian Jiao-tong University and was assigned a lecturer post in 1987. Since 1988, he has been studying at the Free University of Brussels (VUB), Belgium. He received the Special Licentiate in Biomedical and Clinical Engineering, and a Ph.D. in Applied Sciences in 1990 and 1993 respectively. He is currently participating in a project on network communication at VUB. His research interests include information processing in medical imaging, image processing, stereo image analysis, neural nets, and statistical pattern recognition.

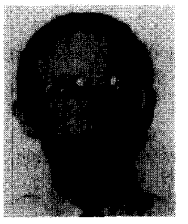

M. Defrise received the Ph.D. degree in theoretical physics from the University of Brussels in 1981, and was a visiting professor in the Department of Radiology of the University of Geneva in 1992–1993. He is currently a senior research associate with the Belgian Science Foundation, and has worked in the Department of Nuclear Medicine at the VUB Hospital in Brussels, Belgium since 1984. In collaboration with groups at Hammersmith Hospital, London and Geneva University Hospital, Switzerland, Dr. Defrise has participated actively in the advancement of 3-D PET methodology. His research interests include 3-D image reconstruction problems in nuclear medicine (PET and SPECT) and in confocal scanning microscopy.

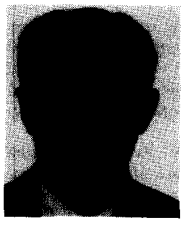

F. Deconinck (M'81) received the Ph.D. degree in physics from the Free University of Brussels (VUB) in 1977. He worked at the University of California at San Francisco and at Brookhaven National Laboratory. Since 1981 he has been a professor at the VUB and is active in the field of information processing in medical imaging as well as in improving access by blind people to graphical computer interfaces, pictorial information, and art.